

Full-Scale Wind Turbine Near-Wake Measurements Using an Instrumented Uninhabited Aerial Vehicle

G. Kocer

e-mail: kocerg@lec.mavt.ethz.ch

M. Mansour

N. Chokani

R.S. Abhari

Laboratory for Energy Conversion,
Department of Mechanical and
Process Engineering, ETH Zurich,
Zurich, CH 8092, Switzerland

M. Müller

MM Engineering,
Hildesheim, DE 31135, Germany

In this paper, the first-ever measurements of the wake of a full-scale wind turbine using an instrumented uninhabited aerial vehicle (UAV) are reported. The key enabler for this novel measurement approach is the integration of fast response aerodynamic probe technology with miniaturized hardware and software for UAVs that enable autonomous UAV operation. The measurements, made to support the development of advanced wind simulation tools, are made in the near-wake ($0.5D$ – $3D$, where D is rotor diameter) region of a 2 MW wind turbine that is located in a topography of complex terrain and varied vegetation. Downwind of the wind turbine, profiles of the wind speed show that there is strong three-dimensional shear in the near-wake flow. Along the centerline of the wake, the deficit in wind speed is a consequence of wakes from the rotor, nacelle, and tower. By comparison with the profiles away from the centerline, the shadowing effects of nacelle and tower diminish downstream of $2.5D$. Away from the centerline, the deficit in wind speed is approximately constant $\approx 25\%$. However, along the centerline, the deficit is $\approx 65\%$ near to the rotor, $0.5D$ – $1.75D$, and only decreases to $\approx 25\%$ downstream of $2.5D$. [DOI: 10.1115/1.4004707]

Keywords: wind energy, wind turbine wake, UAV

1 Introduction

The characteristics of the wake downstream of a wind turbine have an important bearing both on the annual energy yield of a wind farm and on the operation and maintenance costs of the wind turbines within the wind farm. In relation to the former, the annual energy yield, it is well known that the wind speed is reduced in the wake downstream of a wind turbine; the subsequent evolution of the wake is influenced by the topography, and detailed knowledge of this evolution in complex terrain is presently lacking. In regards to the latter, operation and maintenance costs, the wake is characterized by three-dimensionalities and unsteadiness that impact the loads and associated lifecycle of wind turbines. Both of the above factors, the annual energy yield and the operation and maintenance costs, determine the economic viability of a wind farm.

Over the last 25 yr, measurements in the wake of operational full-scale wind turbines have been reported. A radiosonde suspended from a tethered balloon was used to measure the deficit in the hub-height wake velocity up to nine rotor diameters downstream of a 2.5 MW wind turbine [1]. Meteorological towers instrumented with cup anemometers installed at different heights, were used to measure wake velocity profiles one and two-and-half rotor diameters downstream of a 100 kW wind turbine [2]. Kite anemometry was used for measurements in the far-wake (three to nine rotor diameters) of a 2.5 MW wind turbine operating under stable night-time flow conditions [3]. SODAR, Tala kite and meteorological mast measurements in the near- and far-wake regions of a 2 MW wind turbine that was located in flat terrain have been carried out [4]. SODAR measurements of the velocity deficits in the center and boundaries of the wake, two rotor diameters downstream of a 50 kW wind turbine, have been reported [5]. Nine towers, instrumented with bivane anemometers, were located at the same site as Ref. [1] to provide measurements of the wake's characteristics over

distances from two to ten rotor diameters [6]. In complex terrain, a mast instrumented with cup and propeller anemometers at different heights, has been used to measure wake profiles one rotor diameter downstream of a 100 kW wind turbine [7].

While the aforementioned studies have provided useful information concerning the wake of operational full-scale wind turbines, it is evident that the spatial coverage and spatial resolution of the instrumentation that have been employed is limited. Today, there is increasing use of LIDAR profilers in wind energy applications [8–10]. However, LIDAR profilers provide only a one-dimensional (relative to a horizontal coverage area) measurement. On the other hand, for many decades now, aircraft have been used for meteorological studies over distances from 10 m to 10^5 m. The derivation of the equations needed to determine vertical and horizontal winds from aircraft have been detailed [11] and summarized [12]. The measurements of two velocities (the velocity of the aircraft with respect to the Earth, $\vec{V}_{\text{aircraft}}$, and the velocity of the wind with respect to the moving aircraft, \vec{V}_{TAS}) are required to obtain the wind vector with respect to the Earth, \vec{V} , by using the vector sum, $\vec{V} = \vec{V}_{\text{TAS}} + \vec{V}_{\text{aircraft}}$. Meteorological research aircraft generally use GPS and inertial navigation systems (to measure $\vec{V}_{\text{aircraft}}$) and multihole pressure probes (to measure \vec{V}_{TAS}) in order to derive the wind vector. The measurement of the horizontal wind field over large areas has been accomplished using an instrumented research aircraft [13]. Flight manoeuvres to provide in situ calibration of the wind measurement system on a meteorological research aircraft have been described [14]. Furthermore, postflight filtering of the data from GPS and inertial navigation systems have been developed in order to improve the accuracy of an aircraft's measurements [15]. In one approach for a relatively inexpensive measurement, the GPS-derived positions and airspeeds of a sailplane have been used to estimate wind velocities in mountain lee waves [16]. On the other hand, the conceptual basis of using an uninhabited aerial vehicle (UAV) for relatively inexpensive, meteorological measurements has also been proposed [17]. Because of their relatively low cost, high mobility, and robustness, UAVs have become more widely

Contributed by the Solar Energy Division of ASME for publication in the JOURNAL OF SOLAR ENERGY ENGINEERING. Manuscript received January 19, 2011; final manuscript received July 18, 2011; published online October 13, 2011. Assoc. Editor: Spyros Voutsinas.

used for meteorological measurements. Long-term measurements using UAVs have been demonstrated [18]. Using only the GPS-derived airspeed of the UAV, a plane circular flight trajectory has been used to measure wind speed profiles up to an altitude of 2.5 km [19]. Wind vector measurements within the atmospheric boundary layer have been made using a UAV equipped with a nine-hole probe and were compared with LIDAR and SODAR measurements [20]. A UAV, equipped with an autopilot system for autonomous flight and with meteorological sensors was used to measure atmospheric profiles of wind speed and wind direction up to 3500 m above ground [21]. More recently, a UAV equipped with a five-hole probe was used for measurements of wind [22].

In the present work, the first-ever measurements in the near-wake of a full-scale wind turbine using an instrumented UAV are reported. This present work at ETH Zurich on full-scale wind turbines is complemented by dynamically-scaled wind turbine experiments [23] and advanced wind simulation tools [24]. The dynamically-scaled experiments, which are made under controlled flow conditions, and the full-scale experiments provide data for the development of the advanced wind simulation tools that are of interest to the wind industry. The present measurements are made for an operational, modern wind turbine that is, located in moderately complex terrain. Thus, the effects of topography on the structure of the near-wake can be assessed. In Sec. 2, the characteristics of the measurement site and the wind turbine are detailed. The measurement system and measurement approach are also described. Then the near-wake measurements are presented and discussed. The paper then concludes with summary remarks.

2 Experimental Methodology

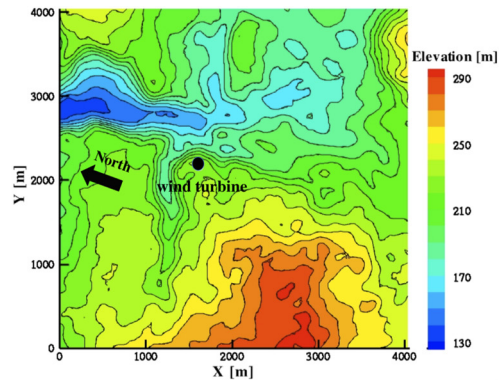
2.1 Site Description and Turbine Characteristics. This field experiment is conducted at a site, which is located in the Weser highland region of northwest Germany. Figure 1 shows the topography of the area. The surface elevations are shown in Fig. 1(a), and it can be seen that in the northwest there is a valley extending approximately in the northwest–southeast direction, and in the east-north-east there is a broad ridge that slopes toward the northwest and south. Figure 1(b) shows the simulated wind flow; the upper plot shows the velocity contours at an elevation of 100 m and in the lower plot are shown the velocity vectors at 10 m elevation. The channelling and acceleration effects of topography on the wind flow are seen in Fig. 1(b). These simulations are obtained with ETH Zurich’s advanced wind simulation tool, which is described in more detail elsewhere [23]. The vegetation of the area is shown in Fig. 1(c); the primary vegetative feature is a covering of open agricultural fields, but includes also a dense grove of small trees. It is evident that because of the effects of the topography and vegetation on the wind flow, the wind turbine at this site operates under the challenging effects of complex terrain.

The 2 MW wind turbine, with a rotor diameter of 80 m atop a 100 m high cylindrical tower, is located as shown in Fig. 1. The automatic yaw control system keeps the rotor faced toward the direction of the incoming wind. Automatic control of the blade pitch maintains a near-constant tip speed ratio. The cut-in and cut-out wind speeds are 4 m/s and 25 m/s, respectively.

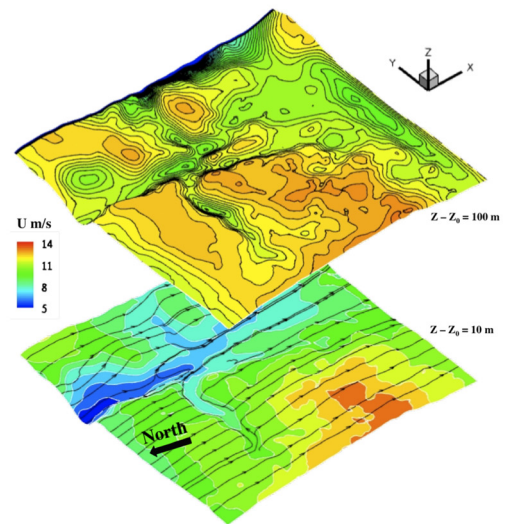
The frequency distribution of the 10-min averaged wind direction and wind speed are shown in Fig. 2. The measurements are from the wind turbine’s nacelle-mounted instrumentation over a 24-h period that includes the duration of the present experiment. The primary wind direction is 280 deg and the average wind speed is 10.4 m/s.

2.2 Measurement System

2.2.1 Instrumented UAV. The unsteady, three-dimensional flowfield around the wind turbine is measured using the instrumented UAV shown in Fig. 3. This electric-powered, pusher-propeller-driven UAV has a wingspan of 800 mm, an overall length of 750 mm and a take-off mass of 900 g. While airborne meteorol-



(a)



(b)



(c)

Fig. 1 Site of the present field experiment. (a) Contours of surface elevation. (b) Simulated wind flow – upper plot shows the velocity contours at an elevation of 100 m and the lower plot the velocity vectors at an elevation of 2 m (c) Vegetative cover. The location of wind turbine is shown in (a) and (c).

ogy has evolved significantly over the past decade, the key enabler for the first-ever measurements in the wake of a full-scale wind turbine, which are reported in this work, is the integration of the fast response aerodynamic probe technology that has been developed at ETH Zurich over the past 20 yr [25] with miniaturized hardware and software for UAVs, that enable autonomous UAV operation [26].

The UAV is instrumented with a seven-sensor fast response probe (7S-FRAP) for measurements of the wind flow. The probe

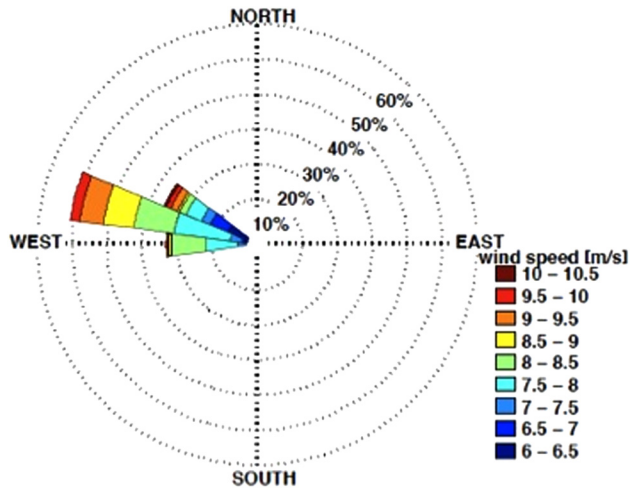


Fig. 2 Frequency distribution of wind speed and wind direction over a 24-h period encompassing the duration of the present field experiment

is described in detail elsewhere [25], but a few salient details are presented here for completeness. The sensing elements of the 7S-FRAP are miniature silicon piezo-resistive chips. These differential pressure sensors are embedded within a 20 mm hemispherical probe head; the probe head is installed on a cylindrical shaft to give an overall probe length of 70 mm. The aerodynamic calibration of the probe was carried out in the fully automated free-jet calibration facility at the Laboratory for Energy Conversion, ETH Zurich [27]. The aerodynamic calibration coefficients determined from the calibration are then used to calculate the dynamic pressure, total pressure and pitch and yaw angles relative to the probe, from which the velocity of the wind with respect to the UAV can



Fig. 3 Instrumented UAV (wingspan, 800 mm) equipped with a seven-sensor fast response aerodynamic probe (diameter, 20 mm)

be determined. The aerodynamic calibration yields less than 0.1% relative error in angles and total pressure. The UAV instrumented with the 7S-FRAP was tested in the low-speed wind tunnel (test-section, 3 m in width \times 2.1 m in height) at the Institute of Fluid Dynamics at ETH Zurich. The wind tunnel tests showed that the measured probe velocities are within the uncertainties of the probe's measurement chain, which is installed in the UAV [28]. The measurement chain of the probe is comprised of the miniature differential pressure sensors, power supplies and signal conditioners, a 14-channel, 24-bit resolution ADC (sampling at 250 Hz), and an onboard multimedia flash card for data storage.

The hardware and software of the open-source autopilot system PAPAARAZZI [26] have been adapted for the present experiments. The hardware suite is comprised of a pressure sensor (VTI Technologies, SCP 1000), temperature sensor (Sensirion, SHT75), GPS (ublox, LEA-5H) and infrared sensors (Melexis, *MLX90247ESF-DSA-ND*). A magnetometer (MicroMag3, #12349) is added to this hardware suite to provide measurements of the UAV's heading.

2.2.2 Uncertainty of Wind Speed Measurements. As described above, the vector sum of the velocity of the UAV with respect to the Earth and the velocity of the wind with respect to the moving UAV are required to obtain the wind vector with respect to the Earth. Thus, the measurement uncertainties of all components in the overall measurement chain are systematically combined using the guide to extended uncertainty in measurements (GUM) [29] to determine the uncertainty in the measurement of the wind vector.

In the GUM method, all sources of uncertainty are modelled as probability distributions, and a Gaussian uncertainty propagation method is used to combine the sources of uncertainty. The GUM method is illustrated in Fig. 4(a) for the aerodynamic calibration of the 7S-FRAP probe. In the present work, the calibration and measurement of components in the overall measurement chain are considered as shown in Fig. 4(b). The GUM method yields a standard uncertainty of 0.7 m/s in the measured wind speed with a confidence level of 67%. The extended uncertainty is used to define error bars shown in the plots of the subsequent results. The measurement chain is still under development, and improvements are underway to further reduce the measurement uncertainty.

2.2.3 Validation of Wind Speed Measurements. The wind measurements of the UAV have been assessed in wind tunnel experiments [28], as described above, and from independent measurements of the UAV flown in circle-flight mode [25]. The circle-flight mode has been used for profiling of the atmospheric boundary layer in meteorology [19,21]. The principle of the circle-flight mode is to fly the UAV in a circle such that the ground speed is decelerated by a headwind on one half of the circle and accelerated by a tailwind on the other half of the circle. If the UAV is operated at a constant true air speed, the wind speed can be determined from the difference between the minimum and the maximum ground speeds over a full circle. Circle-flight mode measurements of wind speed profiles upstream of the wind turbine over heights of $z/z_{\text{hub}} = 0.8\text{--}2.0$ show good agreement with the measurements with the 7S-FRAP probe [25].

For purposes of validation, measurements of the upstream wind, made using the instrumented UAV are compared with measurements from a LIDAR profiler. The LIDAR profiler is a Leosphere Windcube LIDAR system, which operates as a pulsed laser Doppler anemometer. In this system, a pulsed laser beam of 1.54 μm wavelength is used to measure the radial wind speed. To obtain the three-dimensional wind vector, the beam is inclined by 30 deg from the vertical direction and the measurements, at a given height, four different azimuth angles are used to reconstruct the wind vector. The length of the laser pulses, which is approximately 26 m, defines the vertical extent of the measurement, and up to ten different height levels can be measured simultaneously. The LIDAR profiler takes measurements approximately every 1.5 s. The UAV is flown autonomously over the LIDAR at heights, corresponding to measurement heights of the LIDAR. The wind speed profiles

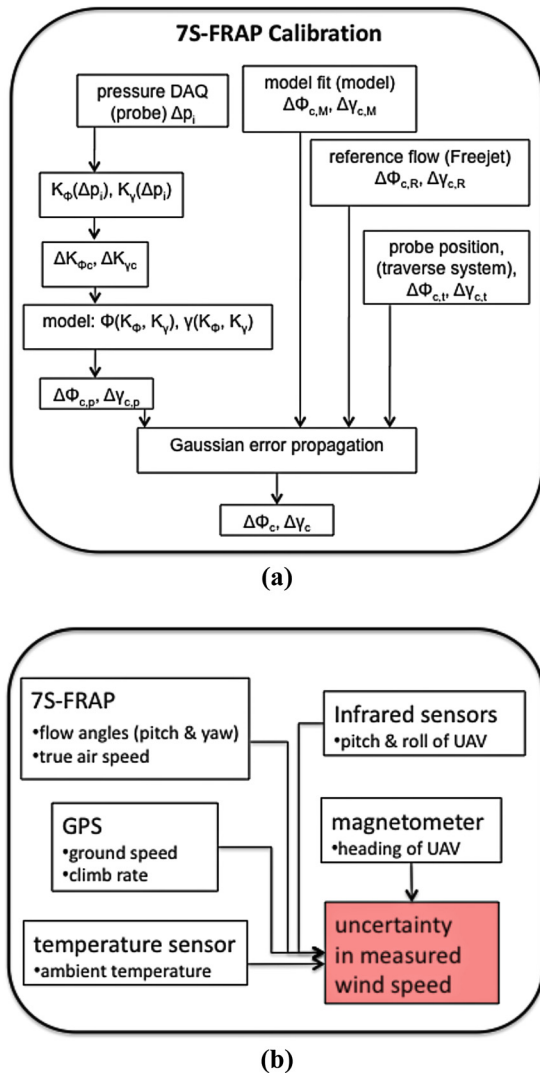


Fig. 4 Sources of uncertainty in measurement of the wind vector. (a) Illustration of the uncertainty propagation using the GUM method to determine the uncertainty in the aerodynamic calibration of the 7S-FRAP probe. (b) Components considered in the calculation of the extended measurement uncertainty of the overall measurement chain.

measured by the UAV are compared with the LIDAR profiler measurements in Fig. 5. In Fig. 5, the wind speed and height are normalized by their respective hub height values. Over the height of measurements, it is seen that there is a good agreement between the UAV and LIDAR profiler measurements.

2.2.4 Measurement Flight Trajectories in the Wake of Wind Turbine. The PAPAZZI software was adapted in order to define trajectories for autonomous flight within a volume that included the wind turbine's wake. The measurements reported here are from a measurement volume that had dimensions of $0.5 < x/D < 3$, $-0.75 < y/D < 0.75$ and $0.6 < z/z_{hub} < 1.6$. Within this volume, 2.5D long, straight, horizontally level, upwind flight segments were autonomously flown between specified start and end waypoints, such as shown in the plan view of Fig. 6; if necessary the waypoints could be adjusted at any time to ensure that the flight segment is aligned with the centerline of the wind turbine's rotor. The offset, in the x - y plane, of successive flight segments was adjusted as desired. Following the upwind flight segment is a sharp left bank turn immediately after end waypoint, then a more gradual turn along an arc of a circle ahead of the start waypoint. The gradual turn ahead of the end waypoint allowed a controlled

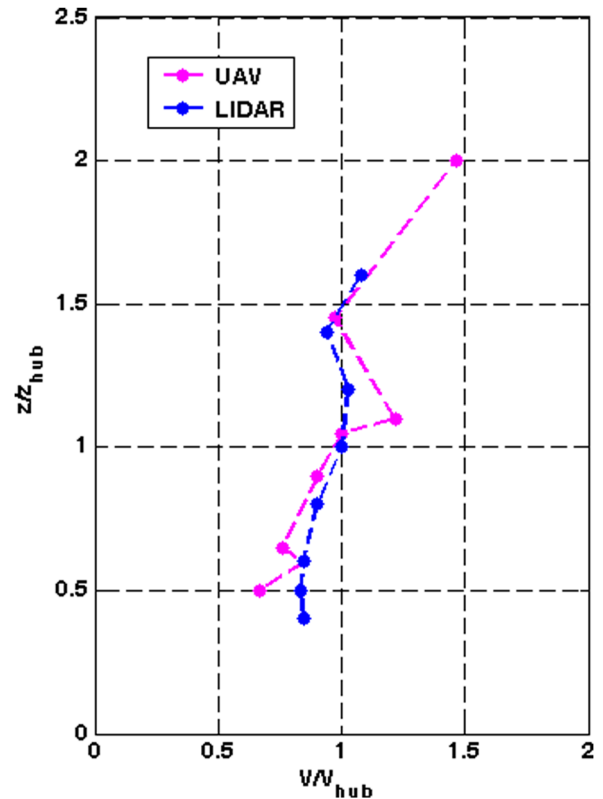


Fig. 5 Comparison of wind speed profiles measured by UAV and LIDAR profiler

ascent to be made to a successive measurement height, if desired; the interval between successive heights is 20 m. The spatial resolution of the measured data is $7.5 \times 10^{-4} D$; in data postprocessing, the resultant wind vector at a given point is derived from 350 successive measured data points; thus in the x - y plane, the measurements in the wake are averaged over 0.25D.

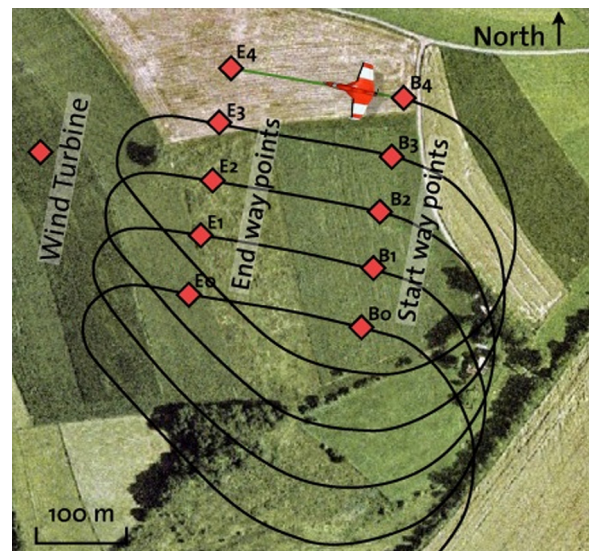


Fig. 6 Plan view of typical flight trajectories of UAV used to measure in the wake of the wind turbine. Symbols B_n and E_n (where $n = 1, 2, \dots, 5$) denote the start and end waypoints of successive measurement segments.

3 Results

The vertical profiles of wind speed upstream of the wind turbine are shown in Fig. 7. The error bars denote the uncertainty in the measured wind speed. The wind speeds are normalised by the upstream hub-height wind speed, V_{ref} . This reference speed is determined, at the time of measurement, from the wind turbine's nacelle-mounted instrumentation [25], and the use of a reference speed in the normalization allows the variations in the ambient wind speed, Fig. 2, to be accounted for. In order to measure the upstream profiles, the UAV is flown from a location 2D upwind of the wind turbine on a straight, horizontal, and upwind flight path over a ground distance of 1.9D. The profiles are for spanwise locations of $y/D = \pm 1.25$. The measured profiles show that there are three-dimensional variations in the flow. There is shear normal to the surface, as is expected, as well as spanwise shear that is due to the topography and vegetative cover shown in Fig 1.

Vertical profiles of wind speed measured downstream of the wind turbine are shown in Fig. 8. The profiles are at streamwise locations of $x/D = 1, 1.5, 2, 2.5,$ and 3 for two spanwise locations of $y/D = 0$, Fig. 8(a), and $y/D = -0.5$, Fig. 8(b). As the UAV's measurement flight trajectory is aligned with the wind turbine's rotor axis, the profiles along $y/D = 0$ show the streamwise evolution along the centerline of the wake, whereas along $y/D = -0.5$ the streamwise evolution away from the centerline is measured. By comparison of the profiles at $x/D = 1$ with the profiles measured upstream of the wind turbine, Fig. 7, the deceleration of the wind speed across the rotor plane, which has a vertical extent of $0.6 < z/z_{hub} < 1.4$ at the centerline, is evident. Above $z/z_{hub} = 1.5$ at $x/D = 1$ for both spanwise locations, there is little variation in wind speed as this region is outside the vertical extent of the wake. Further downstream, $x/D \geq 1$, along the centerline, Fig. 8(a), for $z/z_{hub} > 1.5$, the velocity increases with height; this increase is indicative of the wake's broadening and an increase in the wake's vertical extent as the wake evolves downstream. On the otherhand, over the same streamwise distances away from the centerline, Fig. 8(b), no such broadening is seen; since the rotor's wake has an initially circular cross section at the rotor's plane of rotation, the region $z/z_{hub} > 1.5$, at $y/D = -0.5$, is outside the rotor's wake. Along the centerline, Fig. 8(a), as well as the rotor wake, the profiles at $x/D = 1, 1.5,$ and 2 show the effects of the wakes from the tower and nacelle, as there is a near constant wind speed, $V/V_{ref} \approx 0.4$ for heights $z/z_{hub} < 1.25$ at $x/D = 1$ and 1.5 and $V/V_{ref} \approx 0.5$ for heights $z/z_{hub} < 1$ at $x/D = 2$.

Further downstream, $x/D \geq 2.5$, along the centerline, this region of decelerated flow that is also modified by the tower and

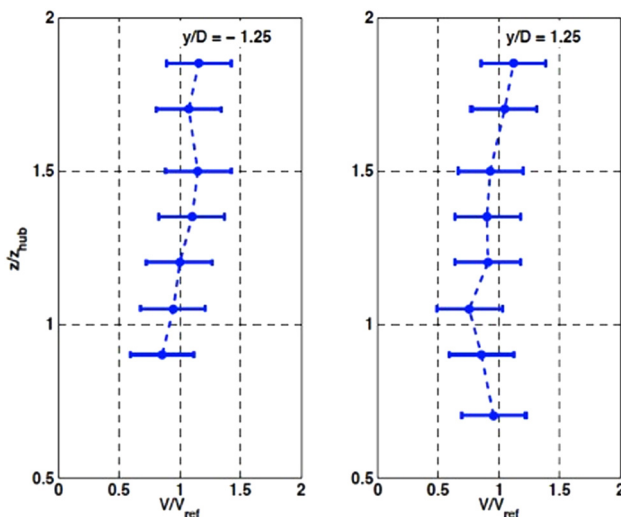


Fig. 7 Profiles of wind speed measured upstream of the wind turbine at spanwise locations of $y/D = \pm 1.25$

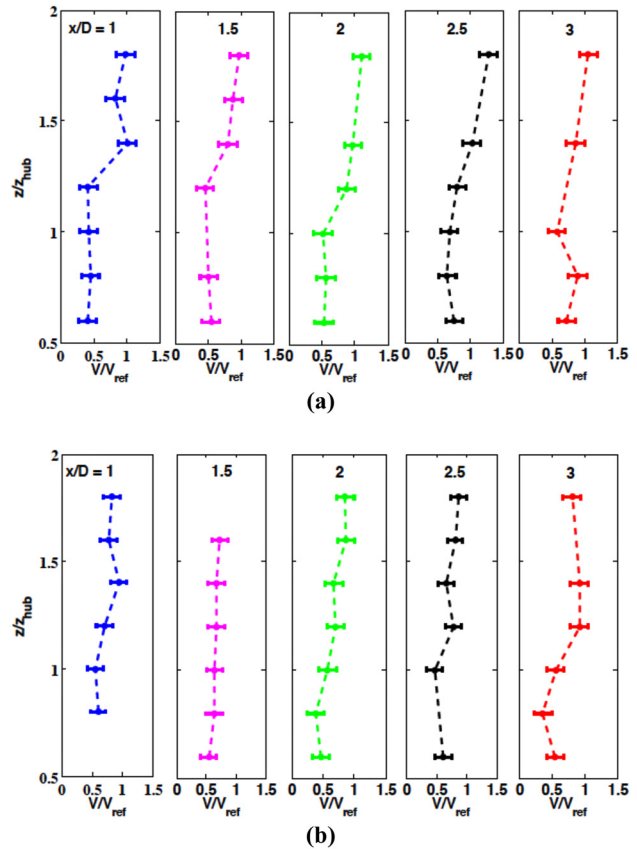


Fig. 8 Profiles of wind speed measured downstream of the wind turbine at streamwise locations of $x/D = 1, 1.5, 2, 2.5,$ and 3 . Profiles are at spanwise locations of (a) $y/D = 0$ and (b) $y/D = -0.5$.

nacelle mixes out. At $x/D = 2.5$, the profile shows that there is a minimum in the wind speed at $z/z_{hub} = 0.8$, which is below the hub height. Further downstream at $x/D = 3$, the minimum wind speed is at hub height. There is also a lower speed observed at $z/z_{hub} = 0.6$, which may be indicative of the vertical shear in the upstream wind profile. Away from the centerline, Fig. 8(b), the flow deceleration is less marked than along the centerline, as at $y/D = -0.5$, there are no shadowing effects of the nacelle and tower. At $x/D = 1$, there is a near constant wind speed, $V/V_{ref} \approx 0.5$ for heights $z/z_{hub} < 1$, and a monotonic increase in the wind speed over the heights $z/z_{hub} = 1-1.4$. Further downstream, $1.5 < x/D < 2.5$, there are variations in the wind speed below hub height. At the most downstream location, $x/D = 3$, the profile shows a distinct minimum in the wind speed, similar to the more upstream profile, $x/D = 2.5$, at the centerline, Fig. 8(a); this is indicative of the increasing horizontal extent of the rotor's wake as the wake evolves downstream.

Profiles of streamwise component of the wind speed measured downstream of the wind turbine are shown in Fig. 9. As described above, an automatic yaw control system aligns the wind turbine with the direction of the upstream wind. The close semblance between the profiles of total and streamwise wind speeds, shown in Figs. 8 and 9, respectively, indicate the efficacy of the yaw control system.

Vertical profiles of the in-plane ($y-z$) component of the wind speed measured downstream of the wind turbine are shown in Fig. 10. The $y-z$ plane is parallel to the rotor plane, and thus the in-plane wind speed components are indicative of the in-plane motion within the wake. Along the centerline, Fig. 10(a), over the vertical extent of the rotor, $0.6 < z/z_{hub} < 1.4$, the magnitude of the in-plane wind speed is initially relatively large,

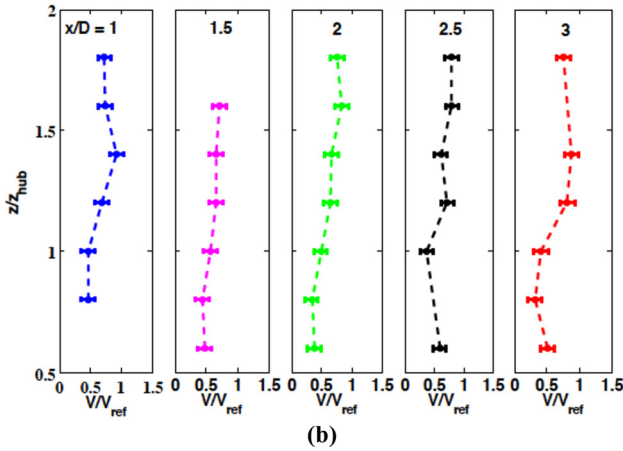
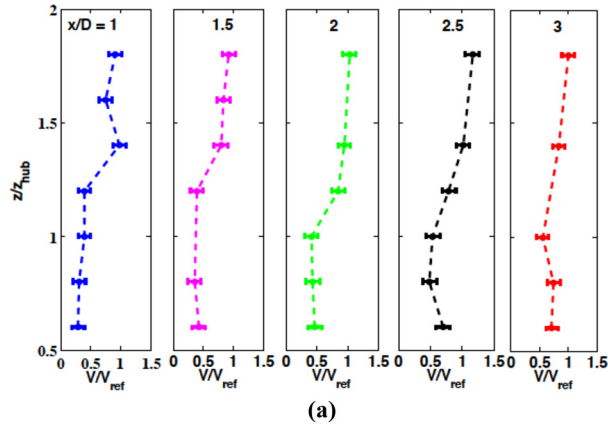


Fig. 9 Profiles of streamwise wind speed measured downstream of the wind turbine at streamwise locations of $x/D = 1, 1.5, 2, 2.5,$ and 3 . Profiles are at spanwise locations of (a) $y/D = 0$ and (b) $y/D = -0.5$.

$V/V_{ref} \approx 0.2$ at $x/D = 1$, and then decreases to relatively small magnitudes, $V/V_{ref} \approx 0$, further downstream at $x/D = 3$. The larger magnitudes are indicative of the flow turning, in-plane rotation and radial broadening of the wake which are all marked occur close to the rotor. Further downstream, these effects diminish due to the mixing out that takes place in the wake, and as in seen in Figs. 9 and 10, the flow is then predominantly in the streamwise direction.

The streamwise evolution of the deficit in hub-height wind speed is shown in Fig. 11. Along the centerline, Fig. 11(a), the deficit is $\approx 65\%$ near to the rotor, $0.5 < x/D < 1.75$; by comparison, at $y/D = -0.5$, away from the centerline, over the same streamwise distance, Fig. 11(c), the deficit is $\approx 25\%$. At an intermediate spanwise position, $y/D = -0.25$, the deficit in wind speed is constant, approximately 40% over $0.5 < x/D < 1.75$. Thus, it is evident that the presence of the tower and nacelle has a marked impact on the deceleration of the flow. Further downstream, $1.75 < x/D < 2.5$, the deficit in wind speed along the centerline, Fig. 11(a), decreases, and for $x/D > 2.5$ deficit is approximately constant $\approx 25\%$. At the mid-span position, $y/D = -0.25$, over the distance, $1.75 < x/D < 3$ the deficit is approximately constant at $\approx 50\%$. Further away from the centerline, Fig. 11(b), over the whole measurement distance, $0.5 < x/D < 3$, the deficit in wind speed is approximately constant $\approx 25\%$. This magnitude of speed deficit is representative of what is expected for rotors of modern wind turbines [30]. The above observations indicate that the impact of the shadowing effect of the tower and the nacelle decreases away from the centerline between $x/D = 0.5$ and 1.75 . However, as is evident from

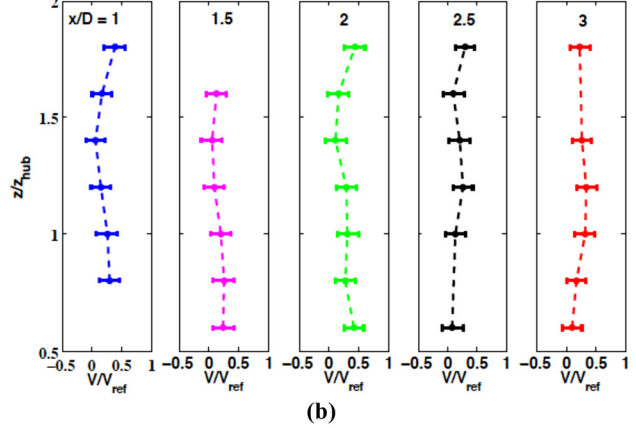
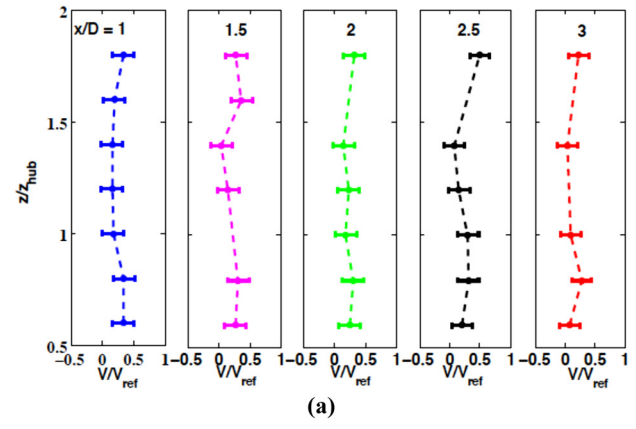


Fig. 10 Profiles of in-plane (y - z) wind speed measured downstream of the wind turbine at streamwise locations of $x/D = 1, 1.5, 2, 2.5,$ and 3 . Profiles are at spanwise locations of (a) $y/D = 0$ and (b) $y/D = -0.5$.

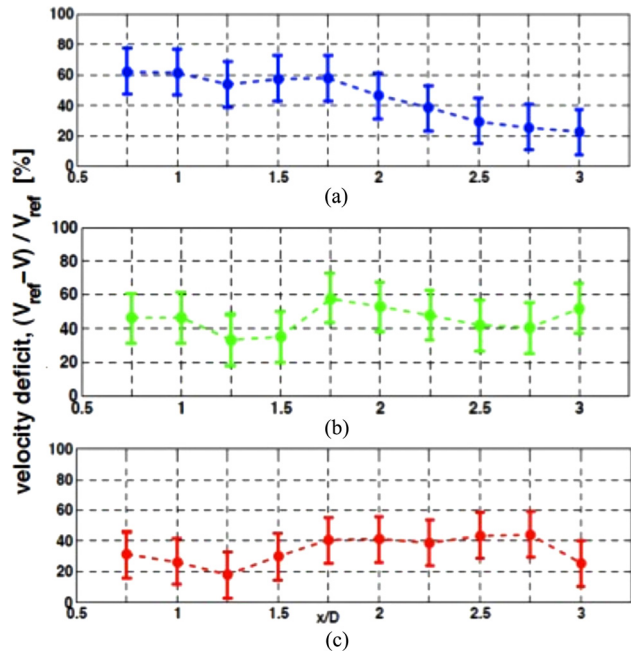


Fig. 11 Streamwise evolution of deficit in hub-height wind speed in the wake. (a) Along centerline ($y/D = 0$), (b) away from centerline ($y/D = -0.25$) and (c) further away from centerline ($y/D = -0.5$).

Fig. 11, in the region $0.5 < x/D < 1.75$ there are strong (25–65%) spanwise variations in the wind speed's deficit that must be accounted for in advanced wind simulation tools.

4 Conclusions

The first-ever measurements in the near-wake of a full-scale wind turbine using an instrumented UAV are reported. The UAV is equipped with a seven-sensor fast response aerodynamic probe; this probe technology has been under development at ETH Zurich for over 20 yr, and allows the measurement of the wind velocity with respect to the UAV. The hardware and software of the open-source autopilot system PAPAARAZZI are used to provide measurement of the UAV's velocity with respect to the Earth; furthermore, PAPAARAZZI is adapted for the planning and execution of autonomous UAV flights within the wind turbine's wake. The vector sum of the UAV's velocity and the wind velocity with respect to the UAV yield the wind vector with respect to the Earth. Application of the guide to extended uncertainty in measurements yields a standard uncertainty of 0.7 m/s in the measured wind speed with a confidence level of 67%. Downwind of the wind turbine, profiles of the wind speed show that there is strong three-dimensional shear in the near-wake flow. Along the centerline of the wake, the deficit in wind speed results from the wakes of the rotor, nacelle and tower. By comparison the profiles away from the centerline, show only the effects of the rotor wake. Away from the centerline, where the wake of the nacelle is absent but the effect of the rotor wake is present, the deficit in wind speed shows little variation with streamwise direction and is approximately constant $\approx 25\%$ in Fig 11(b), over the whole measurement distance, $0.5 < x/D < 3$. However, along the centerline, the deficit is $\approx 65\%$ near to the rotor, $0.5D-1.75D$, and only decreases to $\approx 25\%$ downstream of $2.5D$. These measurements, are used to support the development of advanced wind simulation tools which are currently under development at ETH Zurich.

Acknowledgment

The authors acknowledge the support of Flori Alickaj, Thomas Künzle, and Cornel Reshef at ETH Zurich, in regards to the manufacture of the 7S-FRAP probe and its electronics. The authors gratefully acknowledge the support of Christian Lindenberg, Michael Kislat (from DLR) and Jörg Dittrich (DLR) during the measurement campaign. The authors thank PNE Wind AG for providing access to the wind turbine.

Nomenclature

D	= rotor diameter, 80 m
K	= aerodynamic calibration coefficient of 7S-FRAP probe
M	= model in uncertainty propagation method
p_i	= pressure measured on probe
T	= temperature
V	= speed
\vec{V}	= velocity
x	= streamwise coordinate relative to rotor's plane of rotation
y	= spanwise coordinate relative to rotor's axis of rotation
z	= surface normal coordinate relative to base of wind turbine tower
z_{hub}	= height of wind turbine tower, 100 m

Abbreviations

DAQ	= data acquisition
GPS	= Global Positioning System
LIDAR	= Light Detection and Ranging
SODAR	= Sonic Detection and Ranging
TAS	= true air speed

UAV = uninhabited aerial vehicle
7S-FRAP = seven-sensor fast response aerodynamic probe

Greek Symbols

Δ	= uncertainty
γ	= flow pitch angle
Φ	= flow yaw angle

Subscripts

c	= calibration
hub	= hub height
m	= model
ref	= reference at hub height
R	= reference flow conditions in aerodynamic calibration of 7S-FRAP probe
t	= traversing system used in aerodynamic calibration of 7S-FRAP probe

References

- [1] Zambrano, T. G., and Gyatt, G. W., 1983, "Wake Structure Measurements at the MOD-2 Cluster Test Facility at Goodnoe Hills," *IEEE Proceedings*, Washington, Vol. 130, pp. 562–565.
- [2] Taylor, G. J., 1983, "Wake and Performance Measurements on the Lawson-Tancred 17 m Horizontal-Axis Windmill," *IEEE Proceedings*, Vol. 130, pp. 604–612.
- [3] Baker, R. W., Walker, S. N., 1984, "Wake Measurements Behind a Large Horizontal Axis Wind Turbine Generator," *Sol. Energy*, 33, pp. 5–12.
- [4] Höglström, U., Asimakopoulos, D. N., Kambezidis, H., Helmis, C. G., and Smedman, A., 1988, "A Field Study of the Wake Behind a 2 MW Wind Turbine," *Atmos. Environ.*, 22, pp. 803–820.
- [5] Kambezidis, H. D., Asimakopoulos, D. N., and Helmis, C. G., 1990, "Wake Measurements Behind a Horizontal-Axis 50 kW Wind Turbine," *Solar Wind Technol.*, 7, pp. 177–184.
- [6] Elliott, D. L., and Barnard, J. C., 1990, "Observations of Wind Turbine Wakes and Surface Roughness Effects on Wind Flow Variability," *Sol. Energy*, 45, pp. 265–283.
- [7] Helmis, C. G., Papadopoulos, K. H., Asimakopoulos, D. N., Papageorgas, P. G., and Soilemes, A. T., 1995, "An Experimental Study of the Near-Wake Structure of a Wind Turbine Operating over Complex Terrain," *Sol. Energy*, 54, pp. 413–428.
- [8] Smith, D. A., Harris, M. A., Coffey, S., Mikkelsen, T., Jorgensen, H. E., Mann, J., and Danielian, G., 2006, "Wind LIDAR Evaluation at the Danish Wind Test Site in Hovsore," *Wind Energy*, 9, pp. 87–93.
- [9] Antoniou, I., Courtney, M., Jørgensen, H. E., Mikkelsen, T., von Humerbein, S., Bradley, S., Piper, B., Harris, M., Marti, I., Aristu, M., Foussekis, D., and Nielsen, M. P., 2007, "Remote Sensing the Wind Using LIDARs and SODARs," *Proceedings EWEC*.
- [10] Courtney, M., Wagner, R., Lindelow, P., 2008, "Testing and Comparison of LIDARs for Profile and Turbulence Measurements in Wind Energy," 14th International Symposium for the Advancement of Boundary Layer Remote Sensing, IOP Conference Series: Earth Environmental Science, (1012021).
- [11] Axford, D. N., 1968, "On the Accuracy of Wind Measurements using an Inertial Platform in an Aircraft and an Example of a Measurement of the Vertical Mesoscale of the Atmosphere," *J. Appl. Meteorol.*, 7, pp. 645–666.
- [12] Lenschow, D. H., 1986, "Aircraft Measurements in the Boundary Layer," *Probing the Atmospheric Boundary Layer*, D. H. Lenschow, ed., American Meteorological Society, pp. 39–55.
- [13] Beswick, K. M., Gallagher, M. W., Webb, A. R., Norton, E. G., and Perry, F., 2008, "Application of the Aventura AIMMS20AQ Airborne Probe for Turbulence Measurements During the Convective Storm Initiation Project," *Atmos. Chem. Phys.*, 8, pp. 5449–5463.
- [14] Bögel, W., and Baumann, R., 1991, "Test and Calibration of the DLR Falcon Wind Measuring System by Maneuvers," *J. Atmos. Ocean. Technol.*, 8, pp. 5–18.
- [15] Khelif, D., Burns, S. P., and Friehe, C. A., 1999, "Improved Wind Measurements on Research Aircraft," *J. Atmos. Oceanic Technol.*, 16, pp. 860–875.
- [16] Millane, R. P., Stirling, G. D., Brown, R. G., Zhang, N., Lo, V. L., Enevoldson, E., and Murray, J. E., 2010, "Estimating Wind Velocities in Mountain Lee Waves Using Sailplane Flight Data," *J. Atmos. Oceanic Technol.*, 27, pp. 147–158.
- [17] Holland, G. J., McGeer, T., and Youngren, H., 1992, "Autonomous Aerosondes for Economical Atmospheric Soundings Anywhere on the Globe," *Bull. Am. Meteorol. Soc.*, 73, pp. 1987–1998.
- [18] Holland, G. J., Webster, P. J., Curry, J. A., Tyrell, G., Gauntlett, D., Brett, G., Becker, J., Hoag, R., and Vaglianti, W., 2001, "The Aerosonde Robotic Aircraft: A New Paradigm for Environmental Observations," *Bull. Am. Meteorol. Soc.*, 82, pp. 889–901.
- [19] Ma, S. Q., Chen, H. B., Wang, G., Pan, Y., and Li, Q., 2004, "A Miniature Robotic Plane Meteorological Sounding System," *Adv. Atmos. Sci.*, 21, pp. 890–896.
- [20] Spiess, T., Bange, J., Buschmann, M., and Vörsmann, P., 2007, "First Application of the Meteorological Mini-UAV 'M2AV'," *Meteorol. Z.*, 16, pp. 159–169.

- [21] Reuder, J., Brisset, P., Jonassen, M., Mueller, M., and Mayer, S., 2009, "The Small Unmanned Meteorological Observer SUMO: A New Tool for Atmospheric Boundary Layer Research," *Meteorol. Z.*, **18**, pp. 141–147.
- [22] Van den Kroonenberg, A., Martin, T., Buschmann, M., Bange, J., and Vörsmann, P., 2008, "Measuring the Wind Vector using the Autonomous Mini Aerial Vehicle M2AV," *J. Atmos. Ocean. Technol.*, **25**, 1969–1982.
- [23] Barber, S., Chokani, N., and Abhari, R. S., 2011, "Effect of Wake Flow Non-Uniformity on Wind Turbine Performance and Aerodynamics," ASME-GT2011-46320.
- [24] Jafari, S., Chokani, N., and Abhari, R. S., 2011, "Terrain Effects on Wind Flow: Simulation with an Immersed Boundary Method," ASME-GT2011-46240, 2011.
- [25] Mansour, M., Kocer, G., Lenherr, C., Chokani, N., and Abhari, R. S., 2011, "Seven-Sensor Fast-Response Probe for Full-Scale Wind Turbine Flowfield Measurements," *J. Eng. Gas Turbines Power*, **133**, p. 081601.
- [26] Mueller, M., and Drouin, A., 2007, "Paparazzi - the Free Autopilot. Build your Own UAV," 24th Chaos Communication Congress, December.
- [27] Kupferschmid, P., Köppel, P., Roduner, C., and Gyarmathy, G., 2000, "On the Development and Application of the Fast-Response Aerodynamic Probe System in Turbomachines—Part I: The Measurement System," *ASME J. Turbomach.*, **122**, pp. 505–516.
- [28] Brücker, D., 2010, "Assessment and Improvement of UAV Measurement System," Masters thesis, Laboratory for Energy Conversion, ETH Zurich.
- [29] Behr, T., Kalfas, A. I., and Abhari, R. S., 2006, "A Probabilistic Uncertainty Evaluation Method for Turbomachinery Probe Measurements," Proceedings 18th Symposium on Measuring Techniques in Turbomachinery, Transonic and Supersonic Flow in Cascades and Turbomachines, September.
- [30] Hau, E., 2006, *Wind Turbines: Fundamentals, Technologies, Applications, Economics*, Springer-Verlag, Berlin.